Torque Distribution Strategies for Energy-Efficient Electric Vehicles with Multiple Drivetrains

1 B. Lenzo[1], G. De Filippis[1], A.M. Dizqah[1,2], A. Sorniotti[1], P. Gruber[1], S. Fallah[1], W. De Nijs[3]

[1]University of Surrey, United Kingdom

[2]Coventry University, United Kingdom

[3]Flanders MAKE, Belgium

Abstract – The paper discusses computationally efficient torque distribution strategies for electric vehicles with individually controlled drivetrains, aimed at minimising the overall power losses, while providing the required level of vehicle torque demand and yaw moment. In particular, analytical solutions of the torque control allocation problem are derived under the realistic hypothesis of power loss characteristics of the individual drivetrains being expressed by third order polynomials of the torque demand. The effect of the load transfers in moderate traction/braking and cornering conditions is discussed in detail, as well as the effect of different drivetrains on the front and rear axles. The analytical solution of the control allocation problem is experimentally validated along multiple driving cycles on an electric vehicle with four identical drivetrains. The results of the analytically-derived algorithm are contrasted with those from other two control allocation strategies, based on the off-line numerical solution of the control allocation problem (i.e., a multi-parametric non-linear programming problem) with lower levels of approximation. The experiments show that for the case study vehicle the analytical solution represents a very good compromise between energy efficiency, drivability, computational load, and simple and predictable design of the controller.

Keywords – Electric vehicle; torque distribution; control allocation; power loss; analytical solution; longitudinal and lateral accelerations

1. Introduction

Electric vehicles with multiple and individually controlled drivetrains allow a significant enhancement of the cornering response through direct yaw moment control, also called torque-vectoring. For example, torque-vectoring can lead to higher levels of maximum lateral acceleration in quasi-static conditions, and a significant enhancement of vehicle yaw damping during extreme transients. These benefits, relevant to both humanly-driven and automatically-driven electric vehicles, have already been discussed and experimentally measured in previous papers [1-4].

A typical direct yaw moment controller (see Figure 1) for an electric vehicle with multiple motors usually consists of: i) a reference generator, responsible for defining the target values of the vehicle states, for example the reference yaw rate, r_{ref}, starting from the driver inputs (i.e., the steering wheel angle, δ, and the accelerator and brake pedal positions, p_a and p_b, respectively), and the measured or estimated vehicle states (e.g., vehicle speed and longitudinal acceleration, V and a_x, respectively); ii) a high-level controller, generating the overall traction/braking force and yaw moment demands (F_x^c and M_z^c, respectively) to achieve the reference values of the states. The yaw moment actuation is possible only in the case of two drivetrains on the same axle (the adoption of torque-vectoring differentials is not considered here); and iii) a low-level controller (i.e., the 'control allocator' in Figure 1), which outputs the reference torques, τ_{d_i}, for the individual wheels, corresponding to the values F_x^c and M_z^c from the high-level controller in ii).

With respect to the control layer iii), four-wheel-drive electric vehicles are characterised by actuation redundancy [5-8]. For example, the same traction/braking force demand for the overall vehicle in straight-line conditions can be generated through different front-to-rear wheel torque distributions. In the case of four individually controlled drivetrains, i.e., one drivetrain per wheel, actuation redundancy implies the additional complexity associated with the generation of M_z^c through the distribution of individual yaw moments among the front and rear axles. The individual yaw moments are actuated through different torques on the left and right wheels. The general problem of optimally distributing the reference signals to redundant actuators is called control allocation [9-11].

In particular, for electric vehicles an important possible target of the control allocation algorithm is the minimisation of the power losses.

Several studies discuss the subject of control allocation for energy-efficient electric vehicles. In particular, [2] and [5] analyse the different forms of power loss at the vehicle level, including the contributions associated with the electric motor drive and the transmission system, tyre rolling resistance and tyre slip in longitudinal and lateral directions. A quasi-static model is adopted to assess the performance of different wheel torque distribution criteria. However, given the complexity of the assessed control allocation algorithms and the required state estimators, the analysis in [2] and [5] was not experimentally validated. Many papers, for example [12-18], present advanced control allocation strategies for reducing the motor drive power losses, the tyre slip power losses, or other tyre-related performance indicators. They are based on relatively complex algorithms, which are quite difficult to implement in practice at the industrial level. Moreover, despite the results show energy efficiency benefits in specific tests, these contributions do not analyse the resulting optimal wheel torque distributions in detail. For real vehicle implementations, there is significant need for understanding the physics of the system and, based on this, simple and effective control allocation algorithms should be developed. This objective is consistent with the general trend towards the actual implementation of optimised energy- and vehicle-related control systems [19-23].

In the specific field of electric vehicles with multiple motors, [8] derives the analytical expressions of the power loss characteristics of electric motor drives. The conclusion is that a 50:50 front-to-rear wheel torque distribution should be the most efficient solution for the case of identical drivetrains on the two axles. Nevertheless, in practice the same paper recommends to use the drivetrain/s of a single axle at low torque demands, and a 50:50 front-to-rear torque distribution at medium-high torques, without specifying the threshold for implementing the transition between the two modes. This control policy is indirectly confirmed by the experimental results in [24] and [25], which do not elaborate on them. [26] presents a simple control allocation algorithm for electric vehicles with identical power loss characteristics on the front and rear axles. However, this preliminary study does not consider the fact that the load transfers induced by the longitudinal and lateral accelerations provoke a variation of tyre rolling resistance and slip ratios, and does not discuss the well-needed extension to the case of different front and rear electric drivetrains. This generalisation is quite important, as several car makers (for example, see [27]) are proposing electric vehicles with multiple and different electric motor drives.

This paper significantly extends the preliminary results of [26]. In particular, the main novel contributions are:

- The analytical solution of the control allocation problem for the case of identical drivetrains on the front and rear axles. The analytical solution of the control allocation problem is called explicit control allocation, and is indicated as E-CA in the remainder of the paper;
- The generalisation of the analytical solution of the wheel torque control allocation problem, by including the effect of the load transfers;
- The extension of the analytical solution of the control allocation problem to the case of different electric drivetrains on the two axles;
- The experimental comparison of the performance of the proposed E-CA with other two control allocation strategies based on off-line optimisations, called implicit control allocation (I-CA) and hybrid control allocation (H-CA), and with the consumption values of the same electric vehicle operating in a front-wheel-drive mode and in a four-wheel-drive mode with constant 50:50 front-to-rear wheel torque distribution.

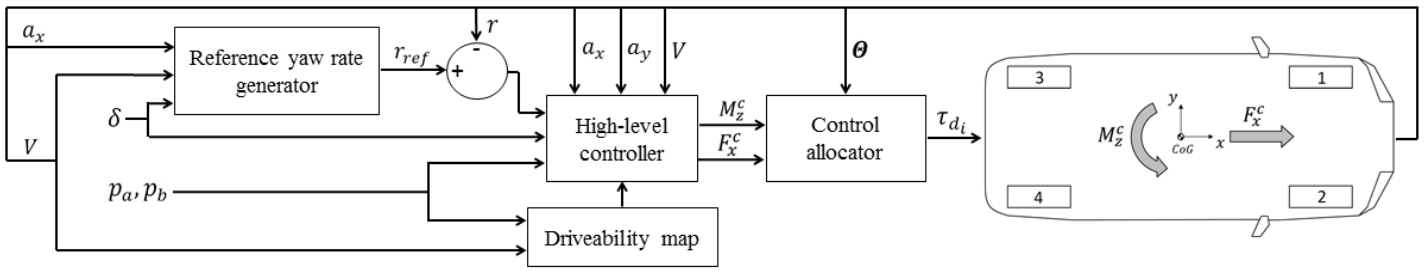

Figure 1 – Simplified schematic of the vehicle control system

2. Problem formulation

2.1 General formulation

The optimal torque distribution among the multiple drivetrains of an electric vehicle can be obtained by solving a multi-parametric nonlinear programming (mp-NLP) problem, which, in general, is formulated as follows [28-29]:

$$\{\boldsymbol{Z}\}^*(\boldsymbol{\Theta}) = \min_{\boldsymbol{X}} J(\boldsymbol{X}, \boldsymbol{\Theta}) \tag{1.a}$$

$$s.t. \quad G(\boldsymbol{X}, \boldsymbol{\Theta}) = 0 \tag{1.b}$$

$$H(\boldsymbol{X}, \boldsymbol{\Theta}) \leq 0 \tag{1.c}$$

where J is the cost function, $\boldsymbol{X}$ is the vector of optimisation variables, $\boldsymbol{\Theta}$ is the vector of parameters, $\{\boldsymbol{Z}\}^*$ is the vector of optimal values, G and H represent the equality and inequality constraint functions, and the symbol $\{\ \}^*$ indicates the optimality of the solution.

The output torque τ_{d_i} of the $i\text{-}th$ drivetrain is defined as:

$$\tau_{d_i} = \tau_{d_{i,t}} - \tau_{d_{i,g}} \tag{2.a}$$

$$\tau_{d_{i,t}} \tau_{d_{i,g}} = 0, \text{ with } i = 1,2,3,4 \tag{2.b}$$

τ_{d_i} is the net drivetrain torque at the wheel, i.e., the torque after the transmission in the case of on-board electric drivetrains. Tyre rolling resistance has to be subtracted from τ_{d_i} to calculate the resultant wheel torque. $\tau_{d_{i,t}} \geq 0$ and $\tau_{d_{i,g}} \geq 0$ are the traction and regeneration torques, respectively. Equality (2.b) has to be imposed because each electric drivetrain can only operate in traction or regeneration. Figure 1 includes a top view of the car indicating the numbering conventions of the vehicle corners.

In order to minimise the electric vehicle power losses, the mp-NLP problem in (1) can be re-formulated as:

$$\{\boldsymbol{\tau}_D\}^*(\boldsymbol{\Theta}) = \arg\min_{\boldsymbol{\tau}_D} J_1(\boldsymbol{\tau}_D, \boldsymbol{\Theta}) = \sum_{i=1}^{4} P_i\left(\tau_{d_i}, \boldsymbol{\Theta}\right) \tag{3.a}$$

$$s.t. \quad \sum_{i=1}^{4} \tau_{d_i} = F_x^c R \tag{3.b}$$

$$d_f\left(\tau_{d_2} - \tau_{d_1}\right) + d_r\left(\tau_{d_4} - \tau_{d_3}\right) = M_z^c R \tag{3.c}$$

$$-\boldsymbol{\tau}_{D,max,g}(\boldsymbol{\Theta}) \leq \boldsymbol{\tau}_D \leq \boldsymbol{\tau}_{D,max,t}(\boldsymbol{\Theta}) \tag{3.d}$$

$$\boldsymbol{\Theta}_{min} \leq \boldsymbol{\Theta} \leq \boldsymbol{\Theta}_{max} \tag{3.e}$$

$\boldsymbol{\tau}_D = \left[\tau_{d_1}, \tau_{d_2}, \tau_{d_3}, \tau_{d_4}\right]^T$ is the vector of the drivetrain output torques, and P_i is the electrical power drawn or regenerated by the $i\text{-}th$ drivetrain. The analysis of $P_i\left(\tau_{d_i}, \boldsymbol{\Theta}\right)$, presented in the next sections, will show that (3) is a non-convex optimisation problem. The vector of parameters $\boldsymbol{\Theta}$ is defined as:

$$\boldsymbol{\Theta} = \left[V, a_x, a_y, \boldsymbol{\Phi}, \boldsymbol{\Lambda}, \boldsymbol{T}\right]^T \tag{4}$$

where V is vehicle speed, a_x is the longitudinal acceleration of the vehicle and a_y is the lateral acceleration. $\boldsymbol{\Phi} = [\varphi_1, \varphi_2, \varphi_3, \varphi_4]$, $\boldsymbol{\Lambda} = [\sigma_1, \sigma_2, \sigma_3, \sigma_4]$ and $\boldsymbol{T} = [T_1, T_2, T_3, T_4]$ are the vectors of slip angles, slip ratios and motor temperatures, respectively.

Eqns. (3.b) and (3.c) are the two equality constraints of the mp-NLP problem, i.e., the longitudinal force and yaw moment balance equations of the vehicle under the approximation of small steering angles. They guarantee that F_x^c and M_z^c, the reference longitudinal force and yaw moment from the high-level controller, are actually generated. d_f and d_r are the front and rear half-tracks, and R is the tyre radius. The inequality constraints in (3.d) and (3.e) are expressed through the vectors $\boldsymbol{\tau}_{D,max,t}(\boldsymbol{\Theta})$, $-\boldsymbol{\tau}_{D,max,g}(\boldsymbol{\Theta})$, $\boldsymbol{\Theta}_{max}$ and $\boldsymbol{\Theta}_{min}$, which represent the maximum and minimum allowed values for $\boldsymbol{\tau}_D$ and $\boldsymbol{\Theta}$.

2.2 Cost function simplification

By assuming that the vehicle operates with limited yaw rate and limited relative slip ratio among the wheels, which is realistic in normal driving conditions, the speed of each vehicle corner can be approximated as V/R. Therefore, $\boldsymbol{\Lambda}$ is excluded from $\boldsymbol{\Theta}$ in this paper. The effect of the slip ratio distribution will be the object of detailed analysis in the future developments of this study, together

with the effect of the slip angles, here omitted from $\boldsymbol{\Theta}$ as well. Under these approximations, the electric power drawn or regenerated by the $i\text{-}th$ drivetrain can be expressed as:

$$P_i = \tau_{d_i}\frac{V}{R} + P_{loss,i}(\tau_{d_i}, \boldsymbol{\Theta}) \tag{5.a}$$

$$P_{loss,i}(\tau_{d_i}, \boldsymbol{\Theta}) = P_{loss,i,t}(\tau_{d_i}, \boldsymbol{\Theta})s(\tau_{d_i}) + P_{loss,i,g}(-\tau_{d_i}, \boldsymbol{\Theta})s(-\tau_{d_i}) \tag{5.b}$$

$$s(\tau_{d_i}) = \begin{cases} 1 & \tau_{d_i} \geq 0 \\ 0 & \tau_{d_i} < 0 \end{cases} \tag{5.c}$$

The terms $P_{loss,i,t}(\tau_{d_i}, \boldsymbol{\Theta})$ and $P_{loss,i,g}(\tau_{d_i}, \boldsymbol{\Theta})$ are the power losses of the $i\text{-}th$ vehicle corner, respectively in traction and regeneration, while $s(\tau_{d_i})$ is the unit step function. This notation is convenient for describing the power loss characteristics, which may be significantly different in traction and regeneration for the same drivetrain.

By substituting (5) into the cost function $J_1(\boldsymbol{\tau}_D, \boldsymbol{\Theta})$ of (3.a), it is:

$$J_1(\boldsymbol{\tau}_D, \boldsymbol{\Theta}) = F_x^c V + \sum_{i=1}^{4} P_{loss,i}(\tau_{d_i}, \boldsymbol{\Theta}) \tag{6}$$

The term $F_x^c V$ is constant for any $\boldsymbol{\tau}_D$, therefore for the purpose of power loss minimisation the expression of the cost function can be simplified into:

$$J_1(\boldsymbol{\tau}_D, \boldsymbol{\Theta}) = \sum_{i=1}^{4} P_{loss,i}(\tau_{d_i}, \boldsymbol{\Theta}) \tag{7}$$

In real-life applications, the individual power loss characteristics of the vehicle corners may be different from each other for several reasons. For example, Section 4 will focus on the power loss differences caused by: i) limited levels of longitudinal and lateral acceleration when the four electric drivetrains are identical; ii) different drivetrains on the front and rear axles, under the simplifying hypothesis of scaled power loss characteristics.

2.3 Independence of vehicle sides

As shown in [14] and [26], the mp-NLP problem in (3) can be solved independently for each side of the vehicle. In particular, by combining the two expressions in (3.b) and (3.c) and assuming $d = d_f = d_r$, it is:

$$\tau_{d,l} = \tau_{d_1} + \tau_{d_3} = 0.5\left(F_x^c - \frac{M_z^c}{d}\right)R \tag{8.a}$$

$$\tau_{d,r} = \tau_{d_2} + \tau_{d_4} = 0.5\left(F_x^c + \frac{M_z^c}{d}\right)R \tag{8.b}$$

where $\tau_{d,l}$ and $\tau_{d,r}$ are the drivetrain output torques on the left- and right-hand sides of the vehicle.

Hence, the new cost function $J_2(\boldsymbol{\tau}_{D,L}, \boldsymbol{\Theta})$ for the left-hand side of the vehicle is defined as:

$$J_2(\boldsymbol{\tau}_{D,L}, \boldsymbol{\Theta}) = P_{loss,1}(\tau_{d_1}, \boldsymbol{\Theta}) + P_{loss,3}(\tau_{d_3}, \boldsymbol{\Theta}) \tag{9}$$

As a consequence, the optimal torque distribution between the left front and left rear drivetrains is the solution of the following mp-NLP problem:

$$\{\boldsymbol{\tau}_{D,L}\}^*(\boldsymbol{\Theta}) = \arg\min_{\boldsymbol{\tau}_{D,L}} J_2(\boldsymbol{\tau}_{D,L}, \boldsymbol{\Theta}) \tag{10.a}$$

$$s.t. \quad -\boldsymbol{\tau}_{D,L,max,g}(\boldsymbol{\Theta}) \leq \boldsymbol{\tau}_{D,L} \leq \boldsymbol{\tau}_{D,L,max,t}(\boldsymbol{\Theta}) \tag{10.b}$$

$$\boldsymbol{\Theta}_{min} \leq \boldsymbol{\Theta} \leq \boldsymbol{\Theta}_{max} \tag{10.c}$$

where $\boldsymbol{\tau}_{D,L} = \left[\tau_{d_1}, \tau_{d_3}\right]^T$ is a vector containing the drivetrain output torques (τ_{d_1} and τ_{d_3}, see the numbering conventions in Figure 1) for the left-hand side of the vehicle, and the vectors $\boldsymbol{\tau}_{D,L,max,t}(\boldsymbol{\Theta})$ and $-\boldsymbol{\tau}_{D,L,max,g}(\boldsymbol{\Theta})$ represent the maximum and minimum allowed values for $\boldsymbol{\tau}_{D,L}$. For the sake of conciseness, the left-hand side notation is used in the rest of the paper, but the same formulations are

applicable to the right-hand side as well.

2.4 Optimal traction-regeneration balance on a vehicle side

This section demonstrates that $J_2(\boldsymbol{\tau}_{D,L}, \boldsymbol{\theta})$ is minimised if both drivetrains on the same side work either in traction or regeneration, under the hypotheses that $P_{loss,i,t/g}\left(\tau_{d_{i,t/g}}, \boldsymbol{\theta}\right)$ is positive and strictly monotonically increasing as a function of $\tau_{d_{i,t/g}}$, i.e., $P_{loss,i,t/g}\left(\tau_{d_{i,t/g}}, \boldsymbol{\theta}\right) > 0$ and $\partial P_{loss,i,t/g}\left(\tau_{d_{i,t/g}}, \boldsymbol{\theta}\right)/\partial \tau_{d_{i,t/g}} > 0$. These hypotheses were experimentally verified for the vehicle demonstrator of Figure 2 (see Section 3), and are confirmed by other studies (for example, see [30]).

Four scenarios can occur:

$$\text{Scenario 1: } \tau_{d_1} \geq 0 \; AND \; \tau_{d_3} \geq 0 \tag{11.a}$$

$$\text{Scenario 2: } \tau_{d_1} < 0 \; AND \; \tau_{d_3} < 0 \tag{11.b}$$

$$\text{Scenario 3: } \tau_{d_1} \geq 0 \; AND \; \tau_{d_3} < 0 \tag{11.c}$$

$$\text{Scenario 4: } \tau_{d_1} < 0 \; AND \; \tau_{d_3} \geq 0 \tag{11.d}$$

Scenarios 1 and 2 represent the pure traction and regeneration cases, while in Scenarios 3 and 4 one drivetrain is in traction and the other one is in regeneration.

Let us suppose that $\tau_{d,l} \geq 0$ and only one drivetrain is active, for example $\tau_{d_1} = \tau_{d,l}$ and $\tau_{d_3} = 0$. By introducing a regenerative torque, $\bar{\tau} > 0$, on the left rear drivetrain, it would be $\tau_{d_{3,new}} = -\bar{\tau}$ and thus $\tau_{d_{1,new}} = \tau_{d,l} + \bar{\tau}$. According to (5), the extra amount of power drawn by the left front electric drivetrain would be $\bar{\tau}\frac{V}{R} + \Delta P_t(\bar{\tau}, \boldsymbol{\theta})$, with respect to the initial case of $\tau_{d_1} = \tau_{d,l}$; the extra amount of power regenerated by the left rear drivetrain would be $\bar{\tau}\frac{V}{R} - \Delta P_g(\bar{\tau}, \boldsymbol{\theta})$, with respect to the initial case of $\tau_{d_3} = 0$. Their difference is positive, i.e., the overall power loss increases. In fact, $\Delta P_t(\bar{\tau}, \boldsymbol{\theta}) = P_{loss,1,t}\left(\tau_{d,l} + \bar{\tau}, \boldsymbol{\theta}\right) - P_{loss,1,t}\left(\tau_{d,l}, \boldsymbol{\theta}\right) > 0$ and $\Delta P_g(\bar{\tau}, \boldsymbol{\theta}) = P_{loss,3,g}(\bar{\tau}, \boldsymbol{\theta}) - P_{loss,3,g}(0, \boldsymbol{\theta}) > 0$, since $P_{loss,i,t/g}$ is positive and strictly monotonically increasing as a function of the respective torque demand.

Similarly, for $\tau_{d,l} < 0$, it results that the introduction of any traction on one of the two left drivetrains would increase the overall power loss on the left-hand side. In conclusion, both drivetrains on the same side must work in either traction or regeneration.

3. Solution of the control allocation problem

3.1 Case study vehicle

The solution of the wheel torque control allocation problem is based on the experimental data obtained during the characterisation of an electric Range Rover Evoque with four identical on-board drivetrains, each of them consisting of a switched reluctance electric motor drive and a single-speed transmission. Table I reports the main vehicle parameters. The experimental tests have been carried out on the MAHA rolling road facility available at Flanders MAKE within the framework of the European project iCOMPOSE [31] (Figure 2).

The experimental power loss characteristics of the left front drivetrain in traction conditions are shown in Figure 3 for different vehicle speeds. The power loss, $P_{loss,1}$, is the difference between the measured electrical power at the inverter and the mechanical power at the roller of the rolling road. As a consequence, the measured power loss characteristics include the losses in the electric motor drive, mechanical transmission and tyre (in the form of rolling resistance and longitudinal slip power losses). The power loss characteristics are expressed as a function of τ_{d_1}, i.e., the left front drivetrain output torque. From a mathematical viewpoint, it is $\tau_{d_1} = \tau_{w_1} + \tau_{RR_1}$. τ_{w_1} is the wheel torque measured by the rolling road sensing system. τ_{RR_1} is the rolling resistance torque, i.e., the torque that has to be applied by the roller to keep the wheel in constant velocity conditions on the rolling road when the electric motor torque of the drivetrain is zero. τ_{RR_1}includes the effects of tyre rolling resistance as well as the drivetrain drag torques occurring in conditions of zero load from the electric motor (for example, the drag torques caused by the windage and churning effects within the gearbox). τ_{RR_1} was experimentally measured by applying zero torque demand to the electric motor drive and imposing the desired level of wheel speed through the roller. In accordance with the theory [32], $\tau_{RR_1}$is a function of vehicle speed. In a first approximation, the quantity $\tau_{RR_1}V/R$ is the rolling resistance power loss, i.e., the value of $P_{loss,1}$ reported for $\tau_{d_1} = 0$ in Figure 3.

The experimental measurements showed good repeatability. For example, the estimated standard deviation of the measured power losses for repeated measurements ranges from 0.60% to 4.67%, where the higher value was obtained at high torques (above 600 Nm). It was also observed that the temperature of the motors does not have significant influence on the results. Based on this, $\boldsymbol{T}$ was removed from $\boldsymbol{\Theta}$ for the specific electric vehicle. Starting from experimental data such as those in Figure 3, the drivetrain torque demand of each corner, i.e., the motor torque demand sent to the inverter multiplied by the transmission gear ratio, was fine-tuned to be coincident with $\tau_{d_i} = \tau_{w_i} + \tau_{RR_i}$.

The solutions of the control allocation problem proposed in this study are based on simplifications of the experimental power loss characteristics. In particular, the main hypothesis behind the E-CA is that, for a given $\boldsymbol{\Theta}$, the power loss characteristic of the $i\text{-}th$ vehicle corner is a cubic polynomial, function of the generic drivetrain output torque τ_d:

$$P_{loss,i}(\tau_d, \boldsymbol{\Theta}) = a_i\,\tau_d^3 + b_i\,\tau_d^2 + c_i\,\tau_d + d_i \tag{12}$$

Figure 2. The vehicle demonstrator set-up on the rolling road facility

TABLE 1
VEHICLE PARAMETERS

Symbol	Name and unit	Value
ℓ	Wheelbase (m)	2.665
τ_{gb}	Gearbox ratio (-)	10.56
R	Wheel radius (m)	0.364
d	Half-track (m)	0.808
–	No. of motors per axle (-)	2
V_{dc}	High-voltage dc bus level (V)	600

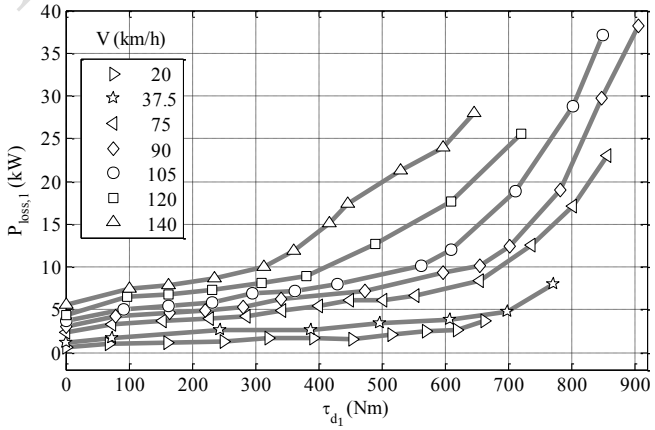

Figure 3. Experimental power loss characteristics for the left front electric drivetrain for different vehicle speeds

By applying (12) to the curves in Figure 3, it can be observed that $a_i, c_i, d_i > 0$, $b_i < 0$, and $b_i^2 < 4a_i c_i$. The physical meaning is that:

- In accordance with the hypothesis in Section 2.4, the characteristics $P_{loss,i}(\tau_d, \boldsymbol{\Theta})$ are strictly monotonically increasing functions of the drivetrain output torque, τ_d. This happens $\forall \tau_d$ if $c_i > 0$, $a_i > 0$ and $b_i^2 < 4a_i c_i$;
- The characteristics $P_{loss,i}(\tau_d, \boldsymbol{\Theta})$ have an inflexion point (see their typical shape in Figure 3) for $\tau_d > 0$, i.e., they exhibit a transition between a non-convex shape and a convex shape for $\tau_d > 0$. An inflexion point exists for $\tau_d > 0$ when $\frac{a_i\, b_i}{|a_i|\,|b_i|} = -1$. Therefore, being $a_i > 0$, it must be $b_i < 0$.

For a vehicle speed of 90 km/h, Figure 4 shows the overlap of: i) the experimental data; ii) a spline-based fitting function [33], used for the I-CA (described in Section 3.3); iii) a linear piecewise fitting function, used for the H-CA (discussed in Section 3.4); and iv) the cubic polynomial fitting function corresponding to Eq. (12), used for the E-CA (discussed in Section 3.2).

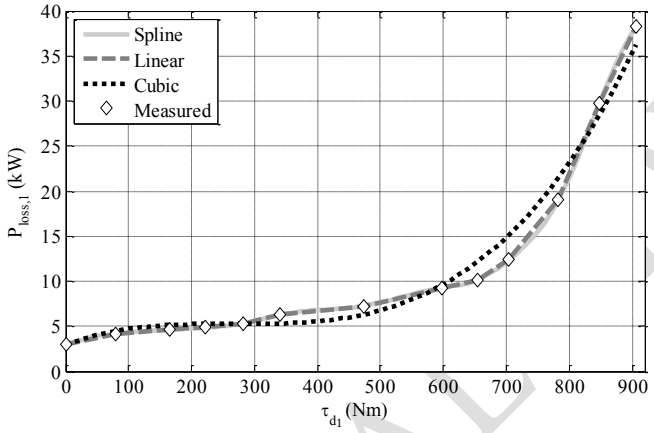

Figure 4. Overlap of the experimental power loss characteristic of the left front drivetrain at 90 km/h and its interpolating functions

3.2 Explicit control allocation (E-CA)

In order to find the analytical solution of the control allocation problem (i.e., the E-CA), the output torques at the left front and left rear drivetrains can be conveniently expressed as:

$$\tau_{d_1} = \tau_0 + \varepsilon \tag{13.a}$$

$$\tau_{d_3} = \tau_0 - \varepsilon \tag{13.b}$$

where ε is the torque shift with respect to the even distribution, i.e., the case of evenly distributed torques among the left front and left rear drivetrains. Hence, $\tau_0 = \tau_{d,l}/2$, which is half of the demanded drivetrain output torque for the left side.

By substituting (13) into (10), the control allocation problem can be reformulated as:

$$\{\varepsilon\}^*(\boldsymbol{\Theta}) = \arg\min_{\varepsilon} J_2(\varepsilon, \tau_0, \boldsymbol{\Theta}) \tag{14.a}$$

$$s.t. \quad -\tau_0 \le \varepsilon \le \tau_0 \tag{14.b}$$

$$\boldsymbol{\Theta}_{min} \le \boldsymbol{\Theta} \le \boldsymbol{\Theta}_{max} \tag{14.c}$$

The expressions of the left front and left rear drivetrain power loss characteristics according to the third order polynomial of Eq. (12) can be substituted into the cost function $J_2(\varepsilon, \tau_0, \boldsymbol{\Theta})$. The result of the calculations is:

$$J_2(\varepsilon, \tau_0, \boldsymbol{\Theta}) = \bar{J}(\varepsilon, \tau_0, \boldsymbol{\Theta}) + (P_{loss,1}(\tau_0, \boldsymbol{\Theta}) + P_{loss,3}(\tau_0, \boldsymbol{\Theta})) = A\,\varepsilon + B\varepsilon^2 + C\varepsilon^3 + (P_{loss,1}(\tau_0, \boldsymbol{\Theta}) + P_{loss,3}(\tau_0, \boldsymbol{\Theta})) \tag{15}$$

where the constant term $P_{loss,1}(\tau_0, \boldsymbol{\Theta}) + P_{loss,3}(\tau_0, \boldsymbol{\Theta})$ is the power loss occurring in the case of even distribution, and the term $A\,\varepsilon + B\varepsilon^2 + C\varepsilon^3$ is the power loss variation induced by the shift ε with respect to the even torque distribution. The coefficients A, B and C in (15) are given by:

$$A = 3\tau_0^2(a_1 - a_3) + 2\tau_0(b_1 - b_3) + c_1 - c_3 \tag{16.a}$$

$$B = 3\tau_0(a_1 + a_3) + b_1 + b_3 \tag{16.b}$$

$$C = a_1 - a_3 \tag{16.c}$$

The minimisation of $J_2(\varepsilon, \tau_0, \boldsymbol{\theta})$ can be achieved by minimising $\bar{J}(\varepsilon, \tau_0, \boldsymbol{\theta})$. By solving $\nabla_\varepsilon \bar{J}(\varepsilon, \tau_0, \boldsymbol{\theta}) = 0$, $\bar{J}$ is minimised by:

$$\bar{\varepsilon} = \frac{-B + \sqrt{B^2 - 3AC}}{3C} \tag{17}$$

while the complementary solution $\frac{-B-\sqrt{B^2-3AC}}{3C}$ is discarded as it maximises $\bar{J}$. If $C = 0$, (17) becomes:

$$\bar{\varepsilon} = \tfrac{-B}{2A} \quad if \quad (C = 0) \quad AND \quad (A \neq 0) \tag{18.a}$$

$$\bar{\varepsilon} = 0 \quad if \quad C = A = 0 \tag{18.b}$$

The solutions in (17-18) minimise $\bar{J}$ only if $B \geq 0$. The optimal value $\{\varepsilon\}^*$ that minimises $\bar{J}$ has to be sought among $\bar{\varepsilon}$, $\varepsilon_{min} = -\tau_0$ and $\varepsilon_{max} = \tau_0$, because $\bar{\varepsilon}$ (if it exists) could be a local minimum or be located outside the domain of ε.

If the vehicle consists of four electric drivetrains with equal power loss characteristics, which, in a first approximation, is true for the vehicle demonstrator in Figure 2, then $P_{loss,i}(\tau_d, \boldsymbol{\theta}) = P_{loss}(\tau_d, \boldsymbol{\theta})$, and thus $A = C = 0$ and $B = 6\tau_0 a_1 + 2b_1$, according to (16) and the fact that $a_1 = a_3$, $b_1 = b_3$, $c_1 = c_3$. In this special case, the optimal solution of (14) for the left-hand side of the vehicle is:

a) $\{\varepsilon\}^* = -\tau_0 \; OR \; \tau_0$, i.e., only one drivetrain should be used for small values of $\tau_{d,l}$ ($B < 0$);
b) $\{\varepsilon\}^* = 0$, i.e., even torque distribution among the drivetrains on the same side should be adopted for large values of $\tau_{d,l}$ ($B \geq 0$);
c) The optimal switching torque, $\tau_{d,SW}$, between strategies a) and b) is calculated as the solution of $B(\tau_0) = 0$:

$$\tau_{d,SW} = 2\,\bar{\tau_0} = -\frac{2(b_1 + b_3)}{3(a_1 + a_3)} = -\frac{2b_1}{3a_1} \tag{19}$$

which is also the solution of the more general expression from [1] (see Theorem 1):

$$P_{loss}(\tau_{d,SW}, \boldsymbol{\theta}) + P_{loss}(0, \boldsymbol{\theta}) = 2P_{loss}\left(\frac{\tau_{d,SW}}{2}, \boldsymbol{\theta}\right) \tag{20}$$

The same results are valid for the right-hand side of the vehicle as well.

3.3 Implicit control allocation (I-CA)

The implicit control allocation (I-CA) is based on an off-line optimisation for the solution of problem (10), to generate the map of the energy-efficient torque distribution for each side of the vehicle. The experimental data of the drivetrain power losses are fitted by means of splines (see Figures 3 and 4), with reduced fitting errors in comparison with the third order polynomial of the E-CA. $r = \frac{\tau_{d_1}}{\tau_{d_1} + \tau_{d_3}}$ is defined as the front-to-total drivetrain torque distribution for the left-hand side of the vehicle, i.e., $r = 1$ or $r = 0$ in the case of single-axle allocation, and $r = 0.5$ in the case of even torque distribution. The resulting I-CA map implemented in this study outputs the optimal front-to-total drivetrain torque ratio, $\{r\}^*$, as a function of vehicle speed and the demanded drivetrain output torque $\tau_{d,s}$ on the specified vehicle side, for example $\tau_{d,s} = \tau_{d,l}$. The map of $\{r\}^*$ can be computed through different optimisation methods, for example Newton-type methods applied to a discretised set of parameters. Figure 5 is the resulting I-CA map for the wheel torque allocation on a vehicle side. Even if the optimal wheel torque distribution according to the I-CA shows more complex behaviour than according to the E-CA, the general trend is towards a single-axle distribution at low torque demands, and an even torque distribution at medium-high torque demands.

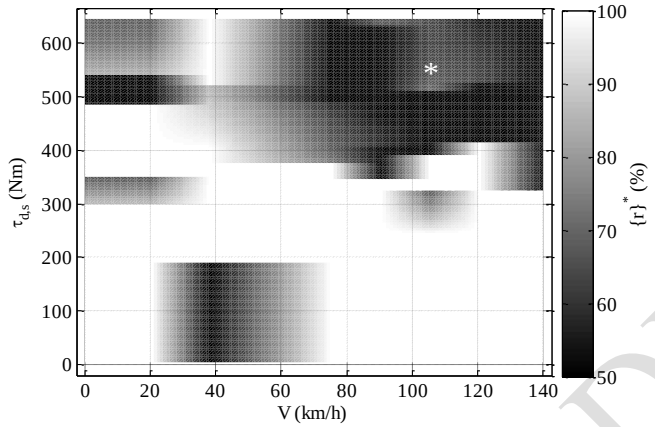

Figure 5. I-CA: map of $\{r\}^*$ as a function of vehicle speed and demanded drivetrain output torque on the vehicle side; the white star represents the point experimentally investigated in steady-state conditions in Section 5

3.4 Hybrid control allocation (H-CA)

The main idea of the hybrid control allocation (H-CA) is to conjugate the simplicity of the E-CA with the high fidelity in the interpolation of the power loss characteristics adopted within the I-CA optimisation. Similarly to the E-CA, the H-CA only allows to move from the single axle to the even distribution by using a single value of the switching torque for a given set of parameters. Similarly to the I-CA, the fitting of the power loss characteristics can be approximated through high-fidelity interpolating functions. The H-CA calculates the switching torque through Eq. (20). In this study a piecewise linear interpolation of the experimental points in Figure 3 is used for the H-CA switching torque calculation.

3.5 Remarks

Based on the experimentally measured power loss characteristics, Figure 6 compares the power loss on the left-hand vehicle side, $P_{loss,s} = P_{loss,1} + P_{loss,3}$, for the single axle strategy (SA, i.e., the whole torque is provided by the front drivetrain), the even distribution strategy (ED), and the I-CA. As expected, for low torque demands SA is more efficient than ED, while it is the opposite at medium-high torque demands. The I-CA provides results that are very close to those of the better among SA and ED for the respective torque demand. This means that the benefit of selecting torque distributions different from single axle or even distribution within a control allocation algorithm is very marginal, with respect to the simple solutions provided by the E-CA and H-CA. Figure 6 shows that the appropriate selection of the front-to-rear torque distribution consistently provides significant energy savings throughout the full range of torques. Figure 7 extends the comparison to the performance of the I-CA, H-CA and E-CA, in decreasing order of energy efficiency, where the differences in terms of power loss among the three control allocation are relatively small, much lower than the differences between the I-CA and the constant distribution strategies in Figure 6.

For completeness, Table 2 compares the switching torque, $\tau_{d,SW}$, calculated for the E-CA and H-CA for the electric Range Rover Evoque demonstrator. The difference in the values is caused by the different fitting functions adopted in the two cases. Although the values in Table 2 for the two strategies are quite far from each other, Figure 7 and the experimental results of Section 5 show that this has a negligible effect in most conditions. For example, at 90 km/h the switching torque, $\tau_{d,SW}$, is 536 Nm for the E-CA and 316 Nm for the H-CA, with a marginal effect, visible in Figure 7, in terms of power loss.

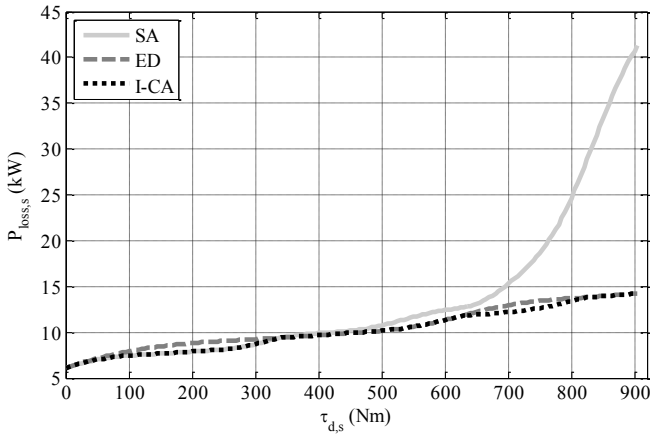

Figure 6. Estimated power losses on a vehicle side at 90 km/h for different torque allocation strategies: single axle (SA), even distribution (ED) and I-CA

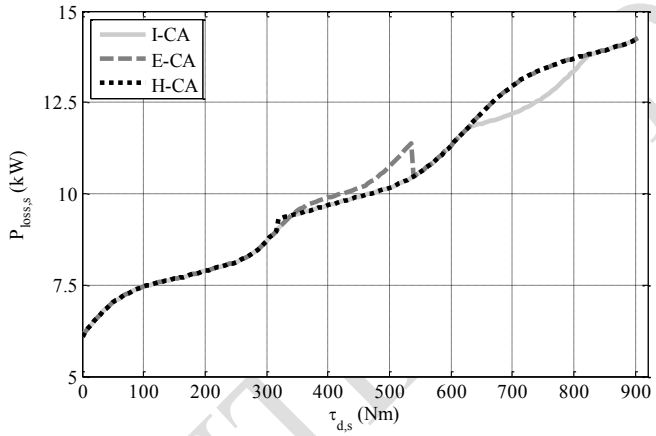

Figure 7. Side power losses at 90 km/h for different torque allocation strategies: I-CA, E-CA and H-CA

TABLE 2
SWITCHING TORQUES AT DIFFERENT VEHICLE SPEEDS:
EXPLICIT CA (E-CA) AND HYBRID CA (H-CA)

$\tau_{d,sw}$	V (km/h)							
(Nm)	0	20	37.5	75	90	105	120	140
E-CA	539	539	626	567	536	525	397	0
H-CA	605	605	605	340	316	281	275	254

4. E-CA: case studies

The following subsections discuss the E-CA solution for the cases of the vehicle subject to moderate load transfers in longitudinal and lateral directions, and the case of different drivetrains on the front and rear axles.

4.1 The effects of the longitudinal and lateral accelerations

Longitudinal and lateral accelerations cause vertical load transfers, which provoke variations of the power loss characteristics of the drivetrains. By using the notations in Figure 7 and neglecting the aerodynamic effects, the vertical loads at each wheel are:

$$F_{z,1} = F_{z0,1} - \frac{1}{2}\Delta F_{z,a_x} - \Delta F_{z,a_y,F} \tag{21.a}$$

$$F_{z,2} = F_{z0,2} - \frac{1}{2}\Delta F_{z,a_x} + \Delta F_{z,a_y,F} \tag{21.b}$$

$$F_{z,3} = F_{z0,3} + \frac{1}{2}\Delta F_{z,a_x} - \Delta F_{z,a_y,R} \tag{21.c}$$

$$F_{z,4} = F_{z0,4} + \frac{1}{2}\Delta F_{z,a_x} + \Delta F_{z,a_y,R} \tag{21.d}$$

where $F_{z0,i}$ is the static load on the $i-th$ wheel, $\Delta F_{z,a_x}$ is the load transfer caused by the longitudinal acceleration a_x, and $\Delta F_{z,a_y,F/R}$ are the lateral load transfers on the front and rear axles, caused by the lateral acceleration a_y. In formulas:

$$\Delta F_{z,a_x} = \frac{m a_x h}{l} \tag{22.a}$$

$$\Delta F_{z,a_y,F/R} = \frac{m a_y}{2d}\frac{a H_{RC,F/R}}{l} + \frac{m a_y}{2d}\frac{k_{\phi_{F/R}}}{k_{\phi_F} + k_{\phi_R}}(h - H_{RC,CoG}) \tag{22.b}$$

The notation $k_{\phi_{F/R}}$ indicates the roll stiffness of the front and rear suspension systems.

Based on [32], the rolling resistance torque is assumed to vary linearly with the vertical load:

$$\tau_{RR_i}(F_{z,i}) = \tau_{RR_i}\left(F_{z_{0,i}}\right)\frac{F_{z,i}}{F_{z_{0,i}}} \tag{23}$$

where $F_{z,i}$ is defined in Eq. (21). As a result, the rolling resistance power loss contribution, $P_{RR_i}(F_{z,i})$, becomes:

$$P_{RR_i}(F_{z,i}) = P_{RR_i}(F_{z_0})\frac{F_{z,i}}{F_{z_{0,i}}} = d_i \tag{24}$$

$P_{RR_i}(F_{z,i})$ is the initial value of $P_{loss,i}$, for $\tau_{d_i} = 0$, i.e., $P_{RR_i}(F_{z,i})$ is the coefficient d_i of the third order polynomial used for the E-CA derivation (see Figures 3 and 4, and Eq. (12)). As a consequence, the variation of vertical load induces a variation of rolling resistance, which provokes a rigid vertical translation of the power loss characteristics, $P_{loss,i}(\tau_{d_i})$, which become different for the four vehicle corners. For example, Figure 9 shows the effects of $a_x = 6$ m/s^2 and $a_y = 2.5$ m/s^2 on the power loss curves of the four drivetrains of the case study electric vehicle demonstrator, at the speed of 90 km/h.

Interestingly, under the hypotheses of the E-CA, in condition of non-zero longitudinal and lateral accelerations the optimal solution of the control allocation problem, $\{\varepsilon\}^*$, is the same as the one derived in Section 3.2, under the hypothesis of identical power loss characteristics for the four vehicle corners. In fact, according to (24), the variation of vertical load affects only the term d_i in Eq. (12). As a consequence, there is no change in the term $\bar{J}$ of Eq. (15), which does not depend on d_i and is actually the only relevant term of the cost function in (15) for the computation of the optimal wheel torque distribution. Based on this important result, a_x and a_y can be removed from $\boldsymbol{\Theta}$, which thus become $\boldsymbol{\Theta} = V$ in this study.

The invariance of the solution is due to the definition of the optimisation problem as a function of the demanded drivetrain output torque, τ_d. If the optimisation problem were defined in terms of $\tau_w = \tau_d - \tau_{RR}$, after appropriate reformulations of the cost function (see Eqns. (13-14)), it would be:

$$\tau_{w_1} = \tau_{w,0} + \varepsilon_w \tag{25.a}$$

$$\tau_{w_3} = \tau_{w,0} - \varepsilon_w \tag{25.b}$$

where $\tau_{w,0}$ is half of the desired wheel torque at the side, e.g., for the left side it is $\tau_{w,0} = (\tau_{w_1} + \tau_{w_3})/2$, while ε_w is the offset from the even wheel torque distribution. By combining $\tau_{d_i} = \tau_{w_i} + \tau_{RR_i}$, Eq. (13) and Eq. (22), it is:

$$\varepsilon_w = \varepsilon + \frac{\tau_{RR_3} - \tau_{RR_1}}{2} \tag{26}$$

which implies that the optimal solution $\{\varepsilon_w\}^*$ depends on the longitudinal and lateral vehicle accelerations, whilst $\{\varepsilon\}^*$ does not.

Figure 10(a) shows the optimal front-to-total torque ratios, $\{r\}^*$, for $a_x = 6$ m/s^2 and $a_y = 2.5$ m/s^2 at 90 km/h. For the same case, Figures 10(b) and 10(c) show $\{\varepsilon\}^*$ and $\{\varepsilon_w\}^*$. From (19), it is $\tau_{d,SW} = 536$ Nm. The switching torque in terms of τ_w is defined as $\tau_{w,SW} = \tau_{d,SW} - \tau_{RR_1} - \tau_{RR_3}$, i.e., $\tau_{w,SW} = 462$ Nm in Figure 10(c).

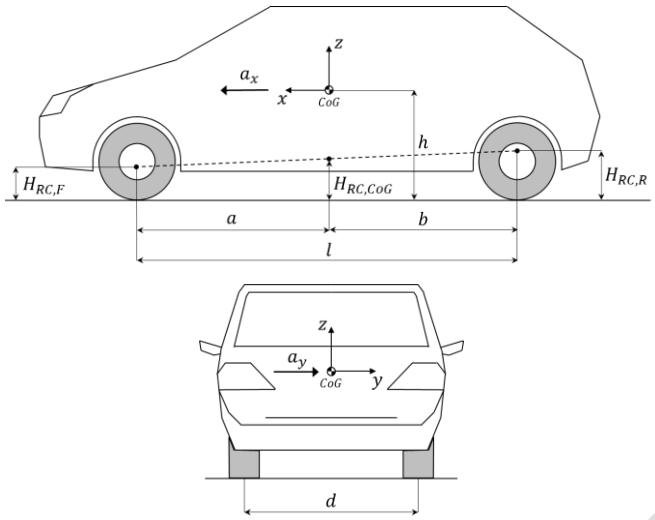

Figure 8. Vehicle schematic with some of the geometric parameters affecting the vertical load transfer caused by longitudinal and lateral accelerations

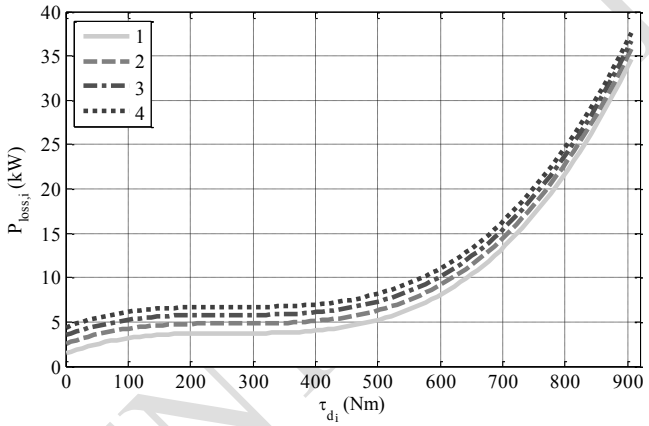

Figure 9. Power loss characteristics at 90 km/h with $a_x = 6$ m/s^2 and $a_y = 2.5$ m/s^2; the values of the subscript i listed in the legend refers to the corner numbering conventions of Figure 1

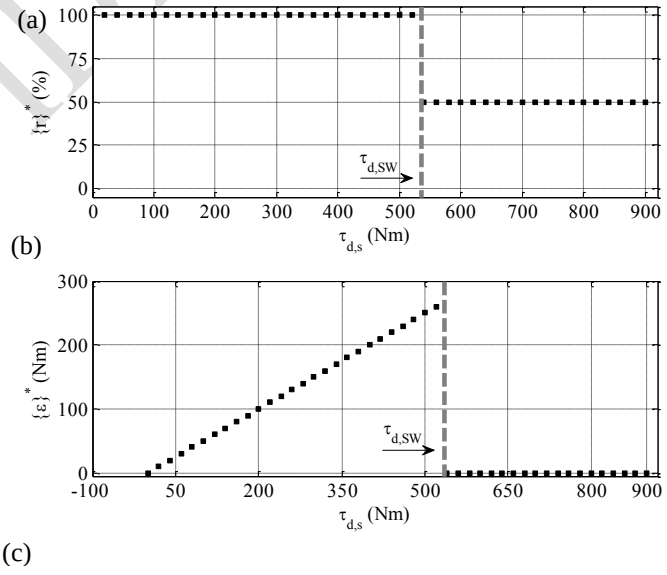

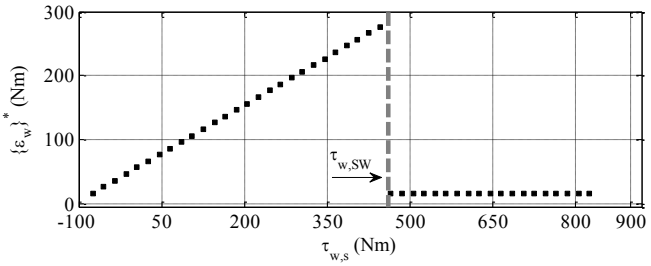

Figure 10. E-CA at 90 km/h with $a_x = 6$ m/s^2 and $a_y = 2.5$ m/s^2: (a) optimal front-to-total torque ratio $\{r\}^*$; (b) optimal torque shift $\{\varepsilon\}^*$; (c) optimal torque shift $\{\varepsilon_w\}^*$

4.2 Different drivetrains on the front and rear axles

The hypothesis of this subsection is that the rear drivetrains have a scaled size with respect to the front drivetrains, i.e., the front and rear drivetrains have the same speed range but they are characterised by different torque ranges. The constant ratio among the maximum torques of the front and rear drivetrains is defined by the scaling factor $\beta > 0$. It is also supposed that the power loss characteristics are scaled according to the same parameter β. This means that the efficiency of the front and rear drivetrains is the same with respect to the normalised torque demand, which is the actual torque divided by the maximum possible value of torque demand for the specific electric drivetrain at the considered speed. This scaling methodology of the efficiency map, already adopted in [34], is not generally applicable, even if it can be realistic and useful in many cases where the drivetrains are different but based on the same motor technology.

From a mathematical viewpoint, on the left-hand side of the vehicle it is:

$$P_{loss,3}(\tau_d, \boldsymbol{\Theta}) = \beta P_{loss,1}(\tau_d/\beta, \boldsymbol{\Theta}) + d_1(1-\beta) \tag{27}$$

The second term in the right-hand side of Eq. (27) allows to maintain the same value of rolling resistance power loss on the two drivetrains, as rolling resistance is not affected by β. In any case, as discussed in the previous section, the rolling resistance power loss does not affect the solution of the control allocation problem. Figure 11 shows the power loss characteristics of the original and scaled drivetrains with $\beta = 0.5$.

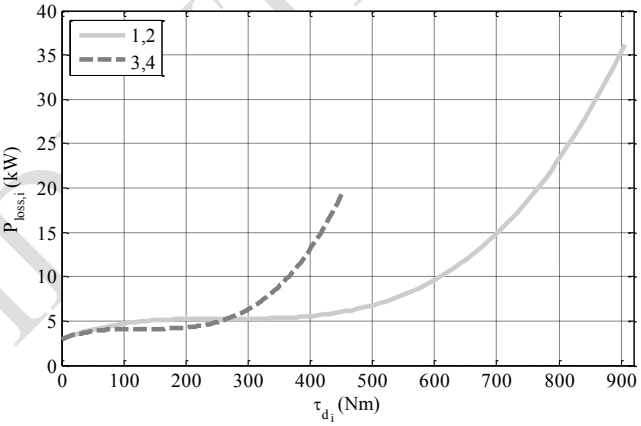

Fig. 11. Power loss characteristics at 90 km/h with $\beta = 0.5$; the values of the subscript i in the legend refer to the corner numbering conventions of Figure 1

By expressing $P_{loss,3}(\tau_d, \boldsymbol{\Theta})$ in the form of a third order polynomial according to Eq. (12) and correlating its coefficients with those of the third order polynomial used for $P_{loss,1}(\tau_d, \boldsymbol{\Theta})$, it results:

$$a_3 = \frac{a_1}{\beta^2},\ b_3 = \frac{b_1}{\beta},\ c_3 = c_1,\ d_3 = d_1 \tag{28}$$

After some re-arrangements, Eq. (17) becomes for the specific case study:

$$\bar{\varepsilon} = \bar{\varepsilon}_1 = \tau_0 \frac{1-\beta}{1+\beta} \quad if \quad \tau_0 \geq \tau_\varepsilon \tag{29.a}$$

$$\bar{\varepsilon} = \bar{\varepsilon}_2 = \tau_0 \frac{1+\beta}{1-\beta} + \frac{2}{3}\frac{b_1}{a_1}\frac{\beta}{1-\beta} \quad if \quad \tau_0 < \tau_\varepsilon \tag{29.b}$$

where:

$$\tau_\varepsilon = -\frac{b_1}{6a_1}(\beta + 1) \tag{30}$$

and the front-to-total torque ratios corresponding to (29.a) and (29.b) are respectively:

$$\bar{r}_1 = \frac{1}{1+\beta} \tag{31.a}$$

$$\bar{r}_2 = \frac{1}{1-\beta} + \frac{b_1}{3a_1\tau_0}\frac{\beta}{1-\beta} \tag{31.b}$$

As discussed in Section 3.2, the optimal solution $\{\varepsilon\}^*$, that is the solution minimising $\bar{J}$, has to be found among the three values $\bar{\varepsilon}$, $-\tau_0$ and τ_0. A procedure to identify $\{\varepsilon\}^*$ among the three options is now presented. In particular, the condition $\bar{J}(-\tau_0) < \bar{J}(\tau_0)$ is satisfied for:

$$\tau_0 \geq \tau_J \quad if \quad \beta \geq 1 \tag{32.a}$$

$$\tau_0 < \tau_J \quad if \quad \beta < 1 \tag{32.b}$$

where:

$$\tau_J = -\frac{b_1}{2a_1}\frac{\beta}{\beta+1} \tag{33}$$

Therefore, the domain of ε can be split into two sub-domains. In the first sub-domain, in which $\bar{J}(-\tau_0) < \bar{J}(\tau_0)$, it is:

$$\{\varepsilon\}^* = \bar{\varepsilon} \qquad if \quad \bar{J}(-\tau_0) \geq \bar{J}(\bar{\varepsilon}) \tag{34.a}$$

$$\{\varepsilon\}^* = -\tau_0 \quad if \quad \bar{J}(-\tau_0) < \bar{J}(\bar{\varepsilon}) \tag{34.b}$$

while in the second sub-domain, in which $\bar{J}(-\tau_0) \geq \bar{J}(\tau_0)$, it is:

$$\{\varepsilon\}^* = \bar{\varepsilon} \quad if \quad \bar{J}(\tau_0) \geq \bar{J}(\bar{\varepsilon}) \tag{35.a}$$

$$\{\varepsilon\}^* = \tau_0 \quad if \quad \bar{J}(\tau_0) < \bar{J}(\bar{\varepsilon}) \tag{35.b}$$

According to (29), $\bar{\varepsilon}$ is $\bar{\varepsilon}_1$ or $\bar{\varepsilon}_2$ depending on the condition $\tau_0 \gtrless \tau_\varepsilon$. Therefore the conditions in (34) and (35) contain four inequalities, concisely $\bar{J}(\pm\tau_0) \geq \bar{J}(\bar{\varepsilon}_{1/2})$. In principle, these inequalities can be expressed in an explicit form, like $\tau_0 \gtrless \hat{\tau}_i$, where the coefficients $\hat{\tau}_i$ are functions of a_1, b_1 and β. Specifically, by defining:

$$\hat{\tau}_A = -\frac{b_1}{2a_1}\frac{\beta+\beta^2}{2\beta+1},\ \hat{\tau}_B = -\frac{b_1}{2a_1}\frac{\beta+1}{\beta+2},\ \hat{\tau}_C = -\frac{b_1}{3a_1}\frac{\beta+\beta^2}{2(2\beta-1)},\ \hat{\tau}_D = -\frac{b_1}{3a_1}\frac{\beta+1}{2(2-\beta)} \tag{36}$$

then, for $\beta < 1$, the following algorithm (Algorithm 1) provides $\{\varepsilon\}^*$. The four external "if" conditions correspond to the four inequalities $\bar{J}(\pm\tau_0) \geq \bar{J}(\bar{\varepsilon}_{1/2})$).

Algorithm 1 – Calculation of $\{\varepsilon\}^*$ for the case of scaled drivetrains among the two axles with $\beta < 1$

```
If τ0 ≥ τε AND τ0 < τJ
  If τ0 ≥ τ̂A AND −τ0 ≤ ε̄1 ≤ τ0
  Then {ε}* = ε̄1, Else {ε}* = −τ0
If τ0 ≥ τε AND τ0 ≥ τJ
  If τ0 ≥ τ̂B AND −τ0 ≤ ε̄1 ≤ τ0
  Then {ε}* = ε̄1, Else {ε}* = τ0
If τ0 < τε AND τ0 < τJ
   If β < 0.5
     If τ0 < τ̂C AND −τ0 ≤ ε̄2 ≤ τ0
     Then {ε}* = ε̄2, Else {ε}* = −τ0
  Elseif β = 0.5
     If −τ0 ≤ ε̄2 ≤ τ0
```

```
    Then {ε}* = ε̄2, Else {ε}* = −τ0
  Elseif β > 0.5
    If τ0 ≥ τ̂C AND −τ0 ≤ ε̄2 ≤ τ0
    Then {ε}* = ε̄2, Else {ε}* = −τ0
If τ0 < τε AND τ0 ≥ τJ
  If τ0 < τ̂D AND −τ0 ≤ ε̄2 ≤ τ0
  Then {ε}* = ε̄2, Else {ε}* = τ0
```

The algorithm and conditions for $\beta > 1$ can be analytically derived as well, and are included in the Appendix.

As discussed in Section 4.1, the longitudinal and lateral accelerations affect only d_i in (18). As a consequence, the optimal solution for non-zero accelerations and scaled drivetrains is identical to the one discussed so far.

Figure 12 shows the optimal front-to-total torque ratio with $\beta = 0.5$ at 90 km/h. The values in Nm are: $\tau_\varepsilon = 201$, $\tau_J = 134$, $\hat{\tau}_A = 151$, $\hat{\tau}_B = 241$, $\hat{\tau}_D = 134$. In the specific case, $\{\varepsilon\}^*$ moves from $-\tau_0$ to τ_0 at $\tau_{d,s} = 2\hat{\tau}_J = 268$ Nm, and then it moves from τ_0 to $\bar{\varepsilon}_1$ ($\bar{r}_1 = 0.67$) at $\tau_{d,s} = 2\hat{\tau}_B = 482$ Nm (note that $\tau_{d,s} = 2\tau_0$).

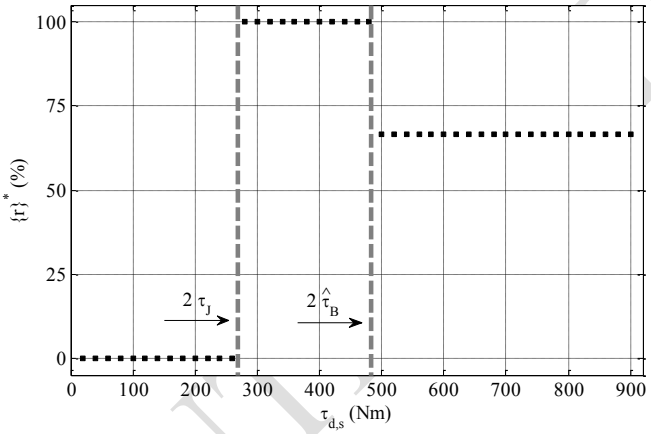

Figure 12. E-CA: optimal front-to-total torque ratio at 90 km/h with $\beta = 0.5$

5. Experimental results

This section reports the main experimental results obtained on the electric Range Rover Evoque demonstrator. The controllers described so far were implemented in real-time on a dSPACE AutoBox system. For the practical operation of the E-CA and H-CA on the vehicle demonstrator, the transition between the single axle and even distribution cases was smoothed by means of appropriate sigmoid functions, in order to provide the required vehicle drivability characteristics. Also, hysteresis functions on the switching thresholds from the single axle to the even distribution cases and vice versa were included to prevent frequent torque distribution oscillations for the E-CA and H-CA. Moreover, in particular conditions, for example during medium-high braking and when the tyre-road friction limits or the drivetrain torque limits are approached, the presented control allocation strategy can be overruled by the electronic brake distribution algorithm, the individual wheel slip controllers or other rule-based algorithms.

Firstly, the effectiveness of the I-CA was verified by means of steady-state rolling road tests at different front-to-total torque ratios, for the same output torque and speed. For example, for the operating point corresponding to the white marker in Figure 5, at $\tau_{d,s}$= 520 Nm and V = 105 km/h, according to the I-CA it is $\{r\}^* = 0.67$. The measured electric motor power inputs with SA, ED and I-CA are 104.82 kW, 102.60 kW and 102.37 kW, where the respective values of the efficiency are 0.7553, 0.7678 and 0.7681. This confirms the correct tuning of the I-CA for steady-state conditions.

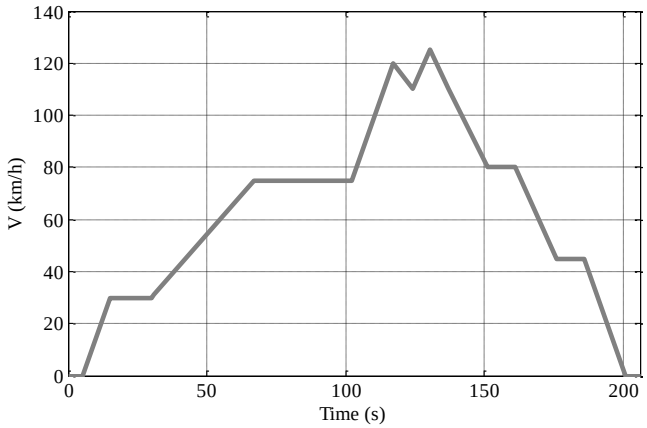

Figure 13. Speed profile of the SDDC

Secondly, the vehicle prototype was tested along four driving cycles: i) the New European Driving Cycle (NEDC); ii) the Artemis Road driving cycle; iii) the Extra Urban Driving Cycle (EUDC, this cycle was run with an emulated uphill constant road slope of 8%); and iv) a newly introduced driving cycle, namely the Surrey Designed Driving Cycle (SDDC). The SDDC was conceived to highlight the effect of the control allocation on the energy consumption, and to assess the difference between E-CA, I-CA and H-CA (see the speed profile in Figure 13 and the operating point distribution in Figure 14). In fact, for the conventional driving cycles in conditions of flat road, the torque distributions chosen by the presented control allocation algorithms tend to be close to the single-axle distribution, because of the very high power rating of the available electric motors. This phenomenon would not occur for an electric vehicle characterised by more conventional power characteristics of the drivetrains. In order to achieve consistency in the results, a driver model, based on the combination of feedforward and feedback control of vehicle speed, was implemented onto the dSPACE system for the computation of the reference torque demand during the driving cycle. As a consequence, the torque demand was electronically imposed during the tests, without a human driver having to control the accelerator and brake pedals.

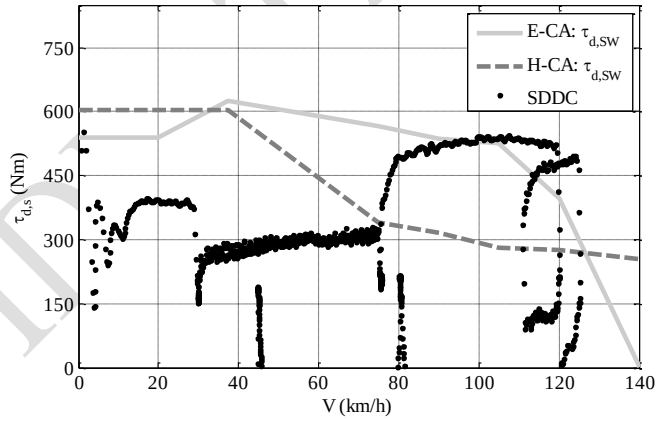

Figure 14. Experimental points of the SDDC and switching torques for E-CA and H-CA

The numerical results of the experiments are reported in Table 3. The main observations are:

- For all driving cycles, the CA strategies lead to reduced energy consumption with respect to the SA and ED;
- For the NEDC, Artemis Road and EUDC the optimal solution is very close either to the SA, for the cycles where the average torque demand level is moderate, or the ED, when the average torque demand level is significant;
- In the SDDC all the control allocation strategies provide a significant improvement (> 2%) with respect to both the SA and ED cases;
- Differently from the steady-state experimental analysis, the I-CA is not the best strategy in actual operating conditions, where it induces continuous fluctuations and transients of the front-to-rear torque distribution. These oscillations compromise vehicle drivability, but also (very marginally) energy efficiency;

- Despite the significant difference among E-CA and H-CA in terms of the switching thresholds for the transition from the single axle operation to the even distribution operation (the thresholds are reported in Figure 14 as functions of speed), the actual difference in the energy consumption results among the two strategies is negligible, with a marginal advantage for the H-CA. This is caused by the fact that for the specific drivetrains there is a relatively wide region of torque demands on each vehicle side where the even torque distribution and single axle torque distribution provide similar power losses.

TABLE 3

ENERGY CONSUMPTION ALONG DRIVING CYCLES WITH DIFFERENT TORQUE ALLOCATION STRATEGIES: SINGLE AXLE (SA), EVEN DISTRIBUTION (ED), IMPLICIT CA (I-CA), EXPLICIT CA (E-CA), HYBRID CA (H-CA)

Driving cycle	Energy consumptions (kWh)					Improvement (%) by I-CA with respect to		Improvement (%) by E-CA with respect to		Improvement (%) by H-CA with respect to	
	SA	ED	I-CA	E-CA	H-CA	SA	ED	SA	ED	SA	ED
NEDC	2.932	3.031	2.921	2.920	2.923	0.38	3.63	0.41	3.66	0.31	3.56
Artemis Road	4.577	4.669	4.549	4.527	4.532	0.61	2.57	1.09	3.04	0.98	2.93
EUDC 8% slope	5.838	5.739	5.730	5.716	5.716	1.85	0.16	2.09	0.40	2.09	0.40
SDDC	1.136	1.141	1.112	1.110	1.103	2.11	2.54	2.29	2.72	2.90	3.33

6. Conclusion

The theoretical and experimental analysis of this paper leads to the following conclusions:

- For the case study electric vehicle a fitting model based on a cubic polynomial is a good approximation of the drivetrain power loss characteristic as a function of the drivetrain torque demand;
- The analytical solution of the control allocation problem can be explicitly achieved from the coefficients of the proposed third order fitting model, including the case of different drivetrains on the front and rear axles, under the hypothesis of scaled power loss characteristics;
- In a first approximation, the load transfer caused by the longitudinal and lateral accelerations provokes a linear variation of the rolling resistance power loss, but it does not change the optimal front-to-total drivetrain torque distribution;
- Tests performed on different driving cycles prove the effectiveness of the explicit control allocation strategy, providing results very close to those of more sophisticated control allocation strategies, the so-called implicit control allocation and hybrid control allocation, requiring off-line numerical optimisations;
- The hybrid control allocation strategy has revealed a slightly higher efficiency with respect to the explicit solution. This result is due to the employment of a fitting model with a lower interpolation error;
- The implicit control allocation strategy allows for a more efficient torque distribution between front and rear axles in steady-state conditions, confirmed by experiments. However, the continuous variation of the torque distribution observed during the driving cycles introduces drivability issues and a marginal increase of the energy consumption;
- The explicit and hybrid control allocation strategies provide a good balance between low on-line computational burden, simple off-line calculations, high energy efficiency during real vehicle operation and good drivability characteristics.

References

1. L. De Novellis, A. Sorniotti, P. Gruber, J. Orus, J.M. Rodriguez Fortun, J. Theunissen and J. De Smet, "Direct yaw moment control actuated through electric drivetrains and friction brakes: Theoretical design and experimental assessment," *Mechatronics*, vol. 26, pp. 1-15, 2015.

2. L. De Novellis, A. Sorniotti and P. Gruber, "Wheel Torque Distribution Criteria for Electric Vehicles With Torque-Vectoring Differentials," *IEEE Transactions on Vehicular Technology*, vol. 63, no. 4, pp. 1593-1602, 2014.

3. Q. Lu et al., "Enhancing vehicle cornering limit through sideslip and yaw rate control," *Mechanical Systems and Signal Processing*, 2016.

4. T. Goggia et al., "Integral sliding mode for the torque-vectoring control of fully electric vehicles: theoretical design and experimental assessment," *IEEE Transactions on Vehicular Technology*, vol. 64, no.5, pp. 1593-1602, 2015.

5. L. De Novellis, A. Sorniotti and P. Gruber, "Optimal wheel torque distribution for a four-wheel-drive fully electric vehicle," *SAE International Journal of Passenger Cars-Mechanical Systems*, 6 (2013-01-0673), pp. 128-136, 2013.

6. Y. Chen and J. Wang, "Adaptive Energy-Efficient Control Allocation for Planar Motion Control of Over-Actuated Electric Ground Vehicles," *IEEE Transactions on Control Systems Technology*, vol. 22, no. 4, pp. 1362-1373, 2014.

7. Y. Suzuki, Y. Kano and M. Abe, "A study on tyre force distribution controls for full drive-by-wire electric vehicle," *Vehicle System Dynamics*, vol. 52, supp. 1, pp. 235-250, 2014.

8. B. Li, A. Goodarzi, A. Khajepour, S.K. Chen and B. Litkouhi, "An optimal torque distribution control strategy for four-independent wheel drive electric vehicles," *Vehicle System Dynamics*, vol. 53, no. 8, pp. 1172-1189, 2015.

9. T.A. Johansen and T.I. Fossen, "Control allocation - A survey," *Automatica*, vol. 49, pp. 1087-1103, 2013.

10. O. Härkegård and S. T. Glad, "Resolving actuator redundancy—optimal control vs. control allocation," *Automatica*, vol. 41, pp. 137-144, 2005.

11. M. Bodson, "Evaluation of optimization methods for control allocation," *Journal of Guidance, Control, and Dynamics*, vol. 25, no. 4, pp. 703-711, 2002.

12. J. Kang, and H. Heo, "Control allocation based optimal torque vectoring for 4WD electric vehicle," *SAE Technical Paper* 2012-01-0246, 2012.

13. L. Xiong and Z. Yu, "Control allocation of vehicle dynamics control for a 4 in-wheel-motored EV," *IEEE Power Electronics and Intelligent Transportation System Conference (PEITS)*, Vol. 2, pp. 307-311. IEEE, 2009.

14. A. Pennycott, L. De Novellis, A. Sabbatini, P. Gruber and A. Sorniotti, "Reducing the motor power losses of a four-wheel drive, fully electric vehicle via wheel torque allocation," *Proceedings of the Institution of Mechanical Engineers, Part D: Journal of Automobile Engineering*, vol. 228, no. 7, pp. 830-839, 2014.

15. X. Yuan and J. Wang, "Torque Distribution Strategy for a Front- and Rear-Wheel-Driven Electric Vehicle," *Vehicular Technology, IEEE Transactions on*, vol. 61, no. 8, pp. 3365-3374, 2012.

16. Y. Chen and J. Wang, "Fast and Global Optimal Energy-Efficient Control Allocation With Applications to Over-Actuated Electric Ground Vehicles," *Control Systems Technology, IEEE Transactions on Control Systems Technology*, vol. 20, no. 5, pp. 1202-1211, 2012.

17. Y. Chen and J. Wang, "Design and Experimental Evaluations on Energy Efficient Control Allocation Methods for Overactuated Electric Vehicles: Longitudinal Motion Case," *IEEE/ASME Transactions on Mechatronics*, vol. 19, no. 2, pp. 538-548, 2014.

18. P. Tøndel and T.A. Johansen, "Control allocation for yaw stabilization in automotive vehicles using multiparametric nonlinear programming," *American Control Conference*, 2005.

19. E. Xydas, C. Marmaras, L.M. Cipcigan, N. Jenkins, S. Carroll and M. Barker, "A data-driven approach for characterising the charging demand of electric vehicles: A UK case study," *Applied Energy*, vol. 162, pp. 763-771, 2016.

20. Z. Dimitrova and F. Maréchal, "Techno–economic design of hybrid electric vehicles and possibilities of the multi-objective optimization structure," *Applied Energy*, vol. 161, pp. 746-759, 2016.

21. W. Shabbir and S.A. Evangelou, "Real-time control strategy to maximize hybrid electric vehicle powertrain efficiency," *Applied Energy*, vol. 135, pp. 512-522, 2014.

22. C. Hou, M. Ouyang, L. Xu and H. Wang, "Approximate Pontryagin's minimum principle applied to the energy management of plug-in hybrid electric vehicles," *Applied Energy*, vol. 115, pp. 174-189, 2014.

23. J.L. Torres, R. Gonzalez, A. Gimenez, and J. Lopez, "Energy management strategy for plug-in hybrid electric vehicles. A comparative study," *Applied Energy*, vol. 113, pp. 816-824, 2014.

24. R. Wang, Y. Chen, D. Feng, X. Huang and J. Wang, "Development and performance characterization of an electric ground vehicle with independently actuated in-wheel motors," *Journal of Power Sources*, vol. 196, no. 8, pp. 3962-3971, 2011.

25. S. Kohler, A. Viehl, O. Bringmann and W. Rosenstiel, "Energy-efficient torque distribution for axle-individually propelled electric vehicles,", IEEE Intelligent Vehicles Symposium, 2014.

26. A.M. Dizqah et al., "A Fast and Parametric Torque Distribution Strategy for Four-Wheel-Drive Energy-Efficient Electric Vehicles," *IEEE Transactions on Industrial Electronics*, 2015.

27. Y. Tang, "Method of operating a dual motor drive and control system for an electric vehicle," US Patent 2013/0241445 A1, 2013.

28. L.F. Domínguez, D.A. Narciso, and E.N. Pistikopoulos, "Recent advances in multiparametric nonlinear programming," *Computers & Chemical Engineering*. 34(5), pp. 707-716, 2010.

29. A. Grancharova, and T.A. Johansen, "Multi-parametric Programming, in Explicit Nonlinear Model Predictive Control - Theory and Applications," Springer: Berlin Heidelberg, pp. 1-37, 2012.

30. C. Lin, Z. Xu, "Wheel torque distribution of four-wheel-drive electric vehicles based on multi-objective optimization," *Energies*, vol. 8, no. 5, pp. 3815-3831, 2015.

31. http://www.i-compose.eu/iCompose/, last accessed on 7th January 2016.

32. G. Genta, Motor vehicle dynamics: modeling and simulation, World Scientific, 1997.

33. C. de Boor, A Practical Guide to Splines, Springer-Verlag, 1978.

34. Di Nicola, F., Sorniotti, A., Holdstock, T., Viotto, F. et al., "Optimization of a Multiple-Speed Transmission for Downsizing the Motor of a Fully Electric Vehicle," *SAE International Journal of Alternative Powertrains*, vol. 1, no. 1, pp. 134-143, 2012.

Appendix

Algorithm 1 – Calculation of $\{\varepsilon\}^*$ for the case of scaled drivetrains among the two axles with $\beta > 1$

If $\tau_0 \geq \tau_\varepsilon$ AND $\tau_0 < \tau_J$
  If $\tau_0 \geq \hat{\tau}_B$ AND $-\tau_0 \leq \bar{\varepsilon}_1 \leq \tau_0$
  Then $\{\varepsilon\}^* = \bar{\varepsilon}_1$, Else $\{\varepsilon\}^* = \tau_0$
If $\tau_0 \geq \tau_\varepsilon$ AND $\tau_0 \geq \tau_J$
  If $\tau_0 \geq \hat{\tau}_A$ AND $-\tau_0 \leq \bar{\varepsilon}_1 \leq \tau_0$
  Then $\{\varepsilon\}^* = \bar{\varepsilon}_1$, Else $\{\varepsilon\}^* = -\tau_0$
If $\tau_0 < \tau_\varepsilon$ AND $\tau_0 < \tau_J$
    If $\beta < 2$
      If $\tau_0 < \hat{\tau}_D$ AND $-\tau_0 \leq \bar{\varepsilon}_2 \leq \tau_0$
      Then $\{\varepsilon\}^* = \bar{\varepsilon}_2$, Else $\{\varepsilon\}^* = \tau_0$
    Elseif $\beta = 2$
      If $-\tau_0 \leq \bar{\varepsilon}_2 \leq \tau_0$
      Then $\{\varepsilon\}^* = \bar{\varepsilon}_2$, Else $\{\varepsilon\}^* = \tau_0$
    Elseif $\beta > 2$
      If $\tau_0 \geq \hat{\tau}_D$ AND $-\tau_0 \leq \bar{\varepsilon}_2 \leq \tau_0$
      Then $\{\varepsilon\}^* = \bar{\varepsilon}_2$, Else $\{\varepsilon\}^* = \tau_0$
If $\tau_0 < \tau_\varepsilon$ AND $\tau_0 \geq \tau_J$
    If $\tau_0 < \hat{\tau}_C$ AND $-\tau_0 \leq \bar{\varepsilon}_2 \leq \tau_0$
    Then $\{\varepsilon\}^* = \bar{\varepsilon}_2$, Else $\{\varepsilon\}^* = -\tau_0$